Inorganic Chemistry

Article

pubs.acs.org/IC

Design, Synthesis, and Optoelectronic Properties of Dendrimeric Pt(II) Complexes and Their Ability to Inhibit Intermolecular Interaction

Hui Li,[†] Jing Li,[†,‡] Junqiao Ding,[†] Wei Yuan,[†,‡] Zilong Zhang,[†] Luyi Zou,[†,§] Xingdong Wang,[†] Hongmei Zhan,*[,†] Zhiyuan Xie,[†] Yanxiang Cheng,[†] and Lixiang Wang[†]

[†]State Key Laboratory of Polymer Physics and Chemistry, Changchun Institute of Applied Chemistry, Chinese Academy of Sciences, Changchun 130022, China

[‡]University of Chinese Academy of Sciences, Beijing 100039, China

[§]State Key Laboratory of Theoretical and Computational Chemistry, Institution of Theoretical Chemistry, Jilin University, Changchun 130023, China

S *Supporting Information*

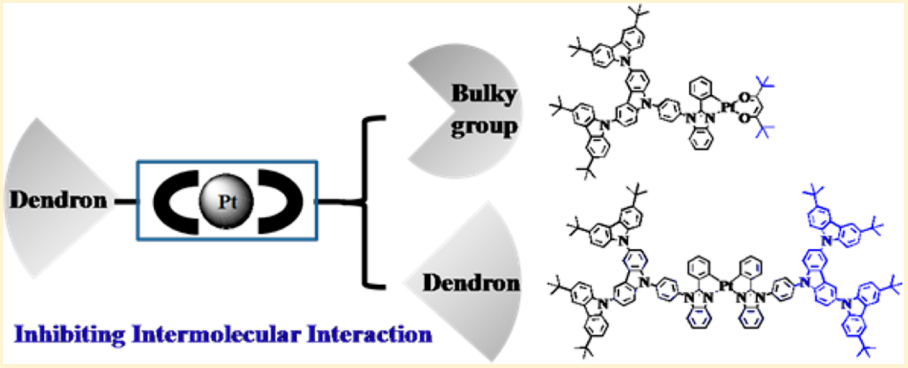

ABSTRACT: Dendrimeric Pt(II) complexes [(C^N)Pt(dpm)] and [Pt(C^N)$_2$] (Hdpm = dipivaloylmethane, HC^N = 1,2-diphenylbenzoimidazole and its derivatives containing the carbazole dendrons) have been synthesized and characterized systematically. All of the complexes display green emission in the range of 495−535 nm that originated from the 360−440 nm absorption bands, which are assigned to dπ(Pt)→π*(L) metal-to-ligand charge transfer (MLCT) mixed with intraligand π(L)→π*(L) transition. Solution photoluminescence quantum yield (φ_p 0.26−0.31) of the heteroleptic complexes [(C^N)Pt(dpm)] obviously increases when compared with that of complex [(C^N)Pt(acac)]. Organic light-emitting diode devices based on these Pt(II) complexes with a multilayer configuration were fabricated and gave desirable electroluminescent (EL) performances, such as non- or less red-shifted EL spectra, in comparison with the photoluminescence spectra and slow efficiency roll-off with increasing brightness or current density. Complex [(*t*-BuCzCzPBI)Pt(dpm)] (where *t*-BuCzCzPBI = 1-(4-(3,6-di-(3,6-di-t-butyl-carbazol-9-yl))carbazol-9-yl)phenyl-2-phenylbenzoimidazole) showed the best performance, with a maximum current efficiency of 29.31 cd/A and a maximum external quantum efficiency (EQE) of 9.04% among the fabricated devices. Likewise, for homoleptic [Pt(*t*-BuCzCzPBI)$_2$] dendrimer, the powder φ_p (0.14) and maximum EQE (0.74%) improve by 7 and 7.4 times, respectively, as high as they do for nondendrimeric [Pt(1,2-diphenylbenzoimidazole)$_2$] (0.02, 0.10%), although its efficiency is still lower than that of the heteroleptic counterpart due to the severely distorted square-planar geometry of the emitting core. These results reveal that large steric hindrance from ancillary ligand (dpm) or the homoleptic conformation can effectively inhibit intermolecular interaction for these dendrimeric Pt(II) complexes.

INTRODUCTION

The study of luminescent Pt(II) complexes has obtained additional momentum since the complexes were found to be efficient as phosphorescent luminophores for harvesting both electrogenerated singlet and triplet excitons to achieve 100% internal quantum efficiency in organic light emitting diodes (OLEDs).[1−4] A recent research effort using blue,[5−12] green,[13−18] red,[19−28] and white[9,13,29−32] phosphorescent Pt(II) complexes based on judiciously chosen ligands has demonstrated the ability to fabricate highly efficient electroluminescent devices. However, Pt(II) complexes have strong axial intermolecular interaction due to their square-planar coordination geometry[33] and always exhibit a tendency to form aggregates or excimers among emissive molecules. The emissions from aggregates/excimers, attributed to metal−

Received: August 18, 2013
Published: January 7, 2014

   dx.doi.org/10.1021/ic402099x | *Inorg. Chem.* 2014, 53, 810−821

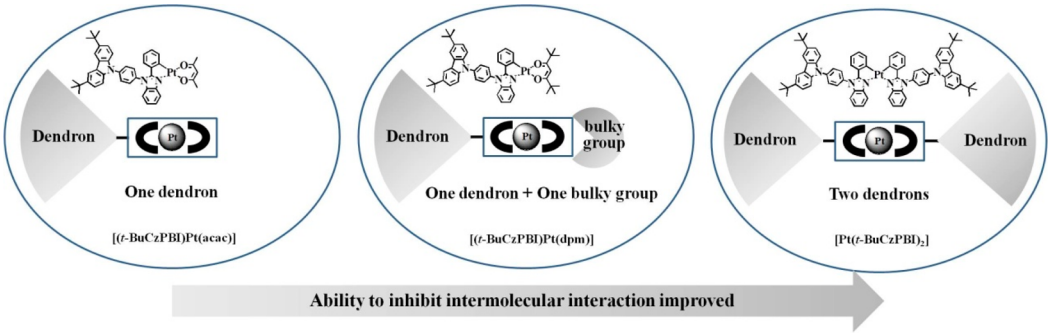

Figure 1. Schematic diagram illustrating molecular structure design.

Scheme 1. (a) Structures of Pt(II) Complexes and (b) Synthetic Route of $[Pt(C^N)_2]$ Complexes

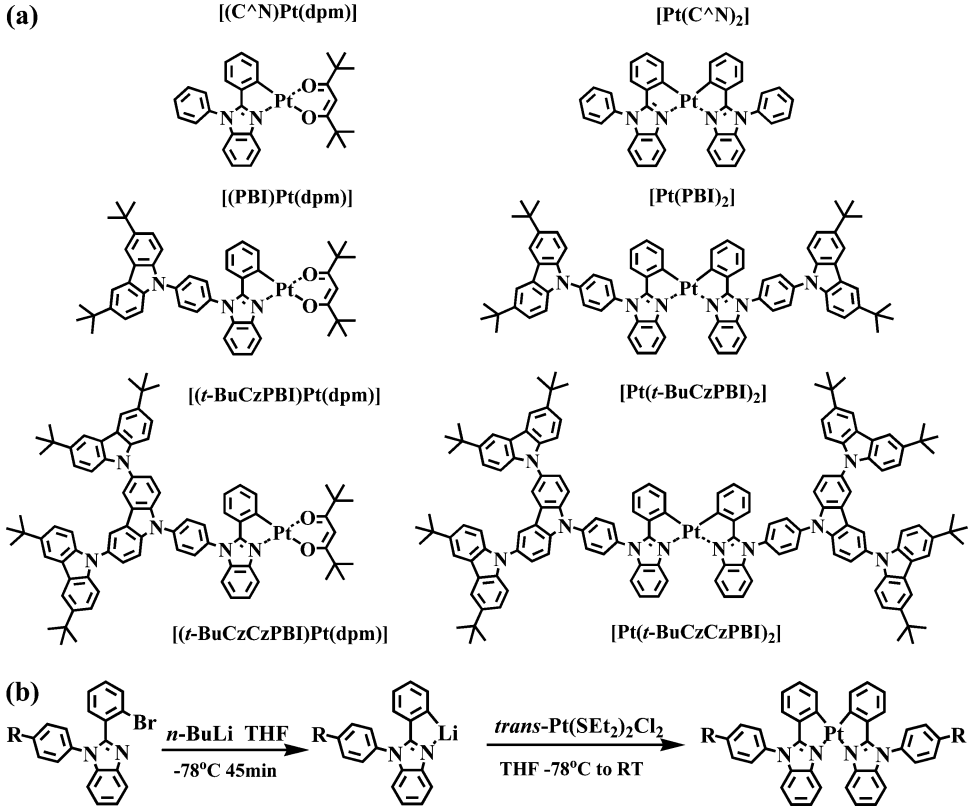

metal-to-ligand charge transfer (MMLCT) or excimeric ligand-to-ligand charge transfer states,[34] can be used to develop simplified single-doped excimer-based white OLEDs,[35−38] but they also result in the occurrence of self-quenching at higher doping concentrations and significantly affect luminescent efficiency, color purity, stability, lifetime, etc.[39,40] Effectively inhibiting the intermolecular interaction by shielding the emitting cores could solve the aforementioned problems and obtain the highly monochromatic emissive Pt(II) complexes.[41] For example, employing rigid and bulky architecture,[42] such as the incorporation of a camphor[43]/trimethylsilane[44]-based substituent, is an effective method. This structure breaks the columnar alignment of complex molecules or weakens the $\pi-\pi$ stacking in the solid state.[45] Accordingly, the Pt(II) complexes exhibit better device performance.[15] In addition, dye encapsulation and steric protection may also prevent the intermolecular interaction by the isolation of the Pt(II) complex molecule. Ikai et al. reported that the "double decamethylene straps" facially encumbered porphyrin Pt(II) complex is more effective in confining triplet excitons and remarkably improved the external quantum efficiency (EQE) values as high as 8.2%.[23] Therefore, the modification of ligand by introducing the functional groups with unique features can, to some extent, successfully suppress the intermolecular interaction of Pt(II) complexes and improve luminescent performance.

Dendrimers with well-defined structure and three-dimensional geometry display the ability to encapsulate emitting core and create specific site-isolated nanoenvironments; they have therefore been applied in phosphorescent organo-transition metal complexes.[46] Corresponding dendrimeric Ir(III), Ru(III), and Re(I) complexes have been successfully explored as OLEDs materials. For instance, the green-emitting OLEDs based on a class of Ir(III) dendrimer, developed by Burn and co-workers, have been prepared with a high current efficiency (CE) of 55 cd/A.[47] Our group has also synthesized carbazole-based dendrimeric green[48] and red[49] Ir(III) emitters with the CE of 45.7 cd/A (EQE 13.4%) and 13.0 cd/A (EQE 11.8%),

dx.doi.org/10.1021/ic402099x | Inorg. Chem. 2014, 53, 810−821

respectively, in which carbazolyl groups act as host material besides encapsulating emitting core and isolating emitting molecules.[46] However, there is still a little doubt that the chemistry of Ir(III) dendrimers is directly applicable to Pt(II) complexes with open coordination sites and fewer coordination numbers,[2] especially the ability to suppress the intermolecular interaction. Recently, the dendrimeric Pt(II) complex [(*t*-BuCzPBI)Pt(acac)] (where *t*-BuCzPBI indicates 1-(4-(3,6-di-t-butylcarbazol-9-yl))phenyl-2-phenylbenzoimidazole and acac indicates the acetylacetonato ligand), reported previously by our group, exhibited an improved CE of 17.55 cd/A (EQE 5.62%), which was 1.6 times as high as that of nondendrimeric [(PBI)Pt(acac)].[50] The increased efficiency illustrated that the dendrons can restrain the formation of aggregates and excimers, but the naked ancillary β-diketonate ligand (acac) of complex [(*t*-BuCzPBI)Pt(acac)] still keeps a great tendency to generate intermolecular interaction at higher concentration (Figure 1), which indicates that further modification work is necessary. In light of this consideration, we designed and synthesized a new series of the dendrimeric Pt(II) complexes, which involved altering the ligand from acac to dipivaloylmethane (dpm) with the bulky *t*-butyl group or adopting the homoleptic conformation to achieve two-sided dendron function (Figure 1). Finally, some beneficial emitting behavior of these dendrimeric Pt(II) complexes in doped matrixes was observed. Using heteroleptic complex [(*t*-BuCzPBI)Pt(dpm)] as a dopant, OLED devices showed a maximum CE of 24.76 cd/A and a maximum EQE of 7.77%, significantly higher than those doped with the [(*t*-BuCzPBI)Pt(acac)] complex. Further extending the size (or generation number) of the dendrons increased the CE and EQE of complex [(*t*-BuCzCzPBI)Pt(dpm)] (where *t*-BuCzCzPBI = 1-(4-(3,6-di-(3,6-di-t-butylcarbazol-9-yl))carbazol-9-yl)phenyl-2-phenylbenzoimidazole) to 29.31 cd/A and 9.04%, respectively. In addition, for homoleptic complex [Pt(*t*-BuCzCzPBI)$_2$], the approach dramatically enhanced its powder photoluminescence (PL) quantum yield and electroluminescent (EL) performance, although the distorted square-planar coordination geometry of the central Pt(II) emitting core affected the efficiency of spin−orbit coupling (SOC),[51] which were thoroughly discussed based on X-ray diffraction analysis and density functional theory (DFT) calculations.

RESULTS AND DISCUSSION

Synthesis and Characterization. The structures and synthetic routes of the new dendrimeric Pt(II) complexes are shown in Scheme 1. The complexes [(C^N)Pt(dpm)] were synthesized by a two-step procedure, referring to previous reports for [(C^N)Pt(acac)] complexes.[5,50] The homoleptic complexes [Pt(C^N)$_2$] were obtained in moderate yield via cyclometalation, as illustrated in Scheme 1b, which involved an in situ generation of the lithiated ligands at low temperature, followed by treatment with a solution of *trans*-Pt(SEt$_2$)$_2$Cl$_2$ (Et = ethyl), a desired Pt(II) precursor, in tetrahydrofuran (THF). The necessary precautions should be adopted in the purification of the objective products because they are photoactive in several solvents such as dichloromethane (DCM) and $CHCl_3$.[52] The formation of [Pt(C^N)$_2$] complexes is completely geometric, and the cis isomers were easily purified. This could be due to the strong steric hindrance of ligands or to the trans effect exerted by the carbon donor atom of the ligated benzene.[2,43] The detailed mechanism for the formation of [*cis*-Pt(C^N)$_2$] complexes was described in the reported literatures.[53,54] All Pt(II) complexes exhibit good solubility in organic solvents, and their structures were verified using ^{1}H and ^{13}C NMR spectroscopy, elemental analysis (EA), and matrix-assisted laser desorption-ionization time-of-flight (MALDI-TOF) mass spectrometry. Their thermal properties were characterized by thermogravimetric analysis (TGA), and the data are summarized in Table 1. These complexes have high thermal stability, and the decomposition temperatures (278−422 °C) are comparable to those of previously reported [(C^N)Pt(acac)] complexes.[50]

The crystal structure of complex [Pt(PBI)$_2$], established by X-ray diffraction (Figure 2), has a nearly cis configuration. The bond distances and angles around the Pt atom are similar to those of reported complexes [Pt(bpy)$_2$], [Pt(bhq)$_2$], and [Pt(thq)$_2$].[51,53,54] The mutual steric congestion between H atoms on C(2) and C(21), C(9) and C(28) [H(2)−H(21) = 3.322 Å, H(9)−H(28) = 3.313 Å] causes sensible distortion of the two ligands in an X-shaped fashion.[51] The Pt atom resides in a deformed square-planar environment with the dihedral angle of 30.9° between the planes of PtC(1)C(6)C(7)N(1) and PtC(20)C(25)C(26)N(3). The large torsion from the ideal square-planar configuration of center Pt(II) emitting core might result in weaker emission for those [Pt(C^N)$_2$] complexes at room temperature (RT).[41]

In the crystal packing, [Pt(PBI)$_2$] molecules stacked as dimers, one molecule of which oriented at a center of inversion relative to the other, and are similar to [(C^N)Pt(acac)] and other Pt(II) species (Figure 2b).[5,50] The shortest Pt−Pt separation was determined to be 7.903 Å, ruling out the presence of any significant Pt−Pt interaction (Figure 2). Part of the overlap between the benzoimidazole fragments in the dimeric units is noted with C atom-to-phenyl separation of 3.579 Å. Other interactions are from *N*-phenyl with the benzoimidazole unit and Pt atom, with the distances of 3.341 and 3.601 Å, respectively. The weak $\pi-\pi$ and d-π interactions, in principle, are unfavorable for emission,[33,39,40,55] which could be suppressed by introducing dendron groups as discussed below in the complexes [Pt(*t*-BuCzPBI)$_2$] and [Pt(*t*-BuCzCzPBI)$_2$] presented in this work.

Photophysical Properties. Figure 3 shows the absorption spectra and the PL spectra of the Pt(II) complexes in DCM, and the corresponding data are listed in Table 1. The other RT and low-temperature (77 K) solution and solid-state emission spectra were recorded for the Pt(II) complexes (Supporting Information, Figures S1−S3). All of the complexes exhibit intense absorption bands below 350 nm that originate from the spin-allowed $\pi\rightarrow\pi^*$ transitions localized on the cyclometalating ligands (^{1}LC), and relatively weak absorption peaks observed in the 360−400 nm region are attributed to spin-allowed singlet d_π(Pt)$\rightarrow\pi^*$(L) metal-to-ligand charge transfer (MLCT) mixed with intraligand π(L)$\rightarrow\pi^*$(L) transition. Weaker absorption shoulders at the long-wavelength tail of each complex are assigned to spin-forbidden ^{3}MLCT transition, which becomes partially allowed due to the strong SOC induced by the Pt heavy metal atom.[25]

Like the absorption properties, the PL spectra of complex [(C^N)Pt(dpm)] are similar to those of the analogous complex [(C^N)Pt(acac)] (Figure 3).[51] Three homologous complexes with dpm ligand show a less vibronically structured RT emission spectra between 497 and 532 nm in DCM solution at 10^{-5} M. Unlike previously reported nondendrimeric Pt(II) complexes,[17,33,41] the shoulder peak, which was produced by intermolecular aggregation, nearly disappeared in the PL

dx.doi.org/10.1021/ic402099x | Inorg. Chem. 2014, 53, 810−821

Table 1. Photophysical, Electrochemical Data, and Decomposition Temperatures for Pt(II) Complexes (Obtained at Room Temperature)

compound	λ_{abs}[a] (log ε) (nm)	λ_{em} (nm)	λ_{em} (nm) [τ(μs)]	φ_p	φ_p [τ(μs)][b]	k_r ($\times 10^5$ s^{-1})[c]	k_{nr} ($\times 10^5$ s^{-1})[c]	HOMO[d] (eV)	LUMO[d] (eV)	ΔE[e] (eV)	T_d[f] (°C)
[(PBI)Pt(acac)][g]	230 (4.8), 247 (4.7), 288 (4.4), 300 (4.5), 313 (4.6), 362 (4.3), 401 (3.7)	494, 527 [6.65]	548 [0.64]	0.25	0.155 [2.82]	5.50	3.00	−5.05	−2.09	2.96	292
[(PBI)Pt(dpm)]	204 (4.2), 216 (4.4), 230 (4.5), 246 (4.5), 289 (4.1), 301 (4.2), 314 (4.3), 366 (4.0), 403 (3.5)	497, 529[a] [1.16][i]	500, 532[h] [4.91]	0.31[i]	0.217 [4.42]	4.91	1.77	−5.54	−2.61	2.93	308
[(t-BuCzPBI) Pt(dpm)]	204 (4.6), 216 (4.7), 234 (4.9), 242 (4.9), 297 (4.6), 314 (4.5), 330 (4.2), 344 (4.2), 366 (4.1), 404 (3.5)	500, 529[a] [1.04][i]	507, 537[h] [2.75]	0.29[i]	0.220 [4.42]	5.19	1.84	−5.51	−2.57	2.94	322
[(t-BuCzCzPBI) Pt(dpm)]	207 (4.8), 218 (5.0), 240 (5.2), 265 (4.9), 288 (4.8), 297 (4.8), 314 (4.6), 333 (4.4), 349 (4.4), 367 (4.2), 404 (3.5)	502, 532[a] [1.47][i]	508, 539[h] [3.82]	0.26[i]	0.204 [3.81]	5.36	2.09	−5.36	−2.41	2.95	302
[Pt(PBI)$_2$]	208 (4.3), 220 (4.5), 232 (4.7), 301 (4.6), 337 (4.1), 393 (4.2), 432 (3.3)	496, 533[j]	517, 543[k] [0.014]	0.02[k]	0.003 [0.58]	0.52	17.34	−5.22	−2.82	2.41	278
[Pt(t-BuCzPBI)$_2$]	215 (4.9), 239 (5.1), 296 (4.8), 309 (4.7), 330 (4.5), 342 (4.4), 394 (4.2), 435 (3.2)	495, 533[j]	514, 540[k] [0.051]	0.03[k]	0.008 [0.20]	3.40	49.20	−5.44	−3.05	2.39	382
[Pt(t-BuCzCzPBI)$_2$]	213 (4.8), 241 (5.3), 265 (4.9), 288 (4.9), 297 (4.9), 333 (4.5), 349 (4.3), 394 (4.0), 436 (3.0)	497, 535[j]	522, 565[k] [0.356]	0.14[k]	0.014 [0.18]	7.76	54.68	−5.28	−2.89	2.39	422

[a]Measured in DCM (10^{-5} M). [b]Measured the film of 30% Pt(II) complexes in poly(methyl methacrylate). [c]The k_r and k_{nr} values are calculated by the following equations, with the assumption that Φ_{ISC} is 1.0. $\Phi_P = \Phi_{ISC}\{k_r/(k_r + k_{nr})\}$; $\tau = (k_r + k_{nr})^{-1}$. [d]Measured in DCM, values were reported versus Fc^+/Fc; ΔE = LUMO − HOMO. [e]Optical band gap. [f]5% mass fraction. [g]Reference 50. [h]Measured the film. [i]Measured in degassed toluene solution. [j]Measured in DCM (10^{-3} M). [k]Measured the powder state.

spectra (Figure 3). Moreover, a small red shift of 121−282 cm^{-1} in film (between 500 and 539 nm) and some enhancement of solution PL quantum yield (φ_p 0.26−0.31) are observed, compared with [(C^N)Pt(acac)] (Supporting Information, Figure S1 and Table 1). These results indicate that the ancillary dpm ligand with bulky *t*-butyl groups does not notably affect the photophysical properties of these [(C^N)-Pt(dpm)] complexes but to some extent does inhibit the unfavorable intermolecular interaction and thus improves their emissive efficiencies.

The homoleptic [Pt(C^N)$_2$] complexes show sharp vibronic progressions of 505, 540, and 584 (shoulder) nm at 77 K, respectively, which is the typical emission from 400 and 433 nm absorptions of complexes, a predominant LC and MLCT triplet state based on the absorption and excitation spectra (Supporting Information, Figure S2). At room temperature, only the weak emissive peaks in the region of 495−535 nm are observed above 10^{-4} M in solution (Figure 3), and nearly nonemissive peaks are observed in the film state because of self-quenching effect (Supporting Information, Figure S4). The SOC effect may be disturbed in severely distorted square-planar [Pt(C^N)$_2$] complexes involving configuration varieties in the excited state.[42] It has been speculated that favorable MLCT states were affected, which will be further discussed in the section of DFT Calculation. However, they exhibit moderately intense emission located at 514−565 nm in powder state (Table 1), and the powder φ_p of complex [Pt(*t*-BuCzCzPBI)$_2$] is 0.14, which is almost 4.6 times that of complex [Pt(*t*-BuCzPBI)$_2$] and 7.0 times that of complex [Pt(PBI)$_2$] (Table 1). The enhanced emissive quantum yield is obviously attributed to the function of two dendrons on both sides. In other words, although these [Pt(C^N)$_2$] complexes exhibit poor phosphorescent emission arising from the distorted emitting core, we can conclude that the homoleptic coordination configuration of Pt(II) dendrimers is able to address the problems produced by open coordination sites of the square-planar Pt(II) complexes, which allow for intermolecular interaction or deactivating pathways with the environment.

DFT Calculation. To understand deeply the fact that weak emission of [Pt(C^N)$_2$] complexes caused by distorted square-planar geometry of the Pt(II) emitting core, DFT calculations on the complexes [Pt(PBI)$_2$] and [(PBI)Pt(acac)], based on X-ray single crystal structure, were carried out. The selected diagrams and data are summarized in Table 2. Their lowest-lying state ($S_0 \rightarrow T_1$) primarily involves the highest occupied molecular orbital (HOMO)→the lowest unoccupied molecular orbital (LUMO) transition {[Pt(PBI)$_2$], 66%; [(PBI)Pt(acac)], 72%}, in which the HOMO is mainly localized at the central Pt(II) atom and the C−H bond-actived phenyl moiety of the C^N ligand, while the LUMO is attributed to delocalized π^* orbital on the PBI ligand. Moreover, the contribution of d orbital electron density (%) of Pt metal in the [Pt(PBI)$_2$] complex is larger than that of the complex [(PBI)Pt(acac)] for HOMO, and smaller for LUMO. In addition, homoleptic [Pt(C^N)$_2$] dendrimers possess stronger ability to suppress the intermolecular interaction. Therefore, the homoleptic [Pt-(C^N)$_2$] dendrimers would show stronger emission, compared with heteroleptic [(C^N)Pt(acac)] species in theory. However, these results are inconsistent with the experimental results, which show that the [(PBI)Pt(acac)] complex is a stronger emitter than the [Pt(PBI)$_2$] complex at RT. A contrast between the two complexes is the coordination geometry: complex

dx.doi.org/10.1021/ic402099x | Inorg. Chem. 2014, 53, 810−821

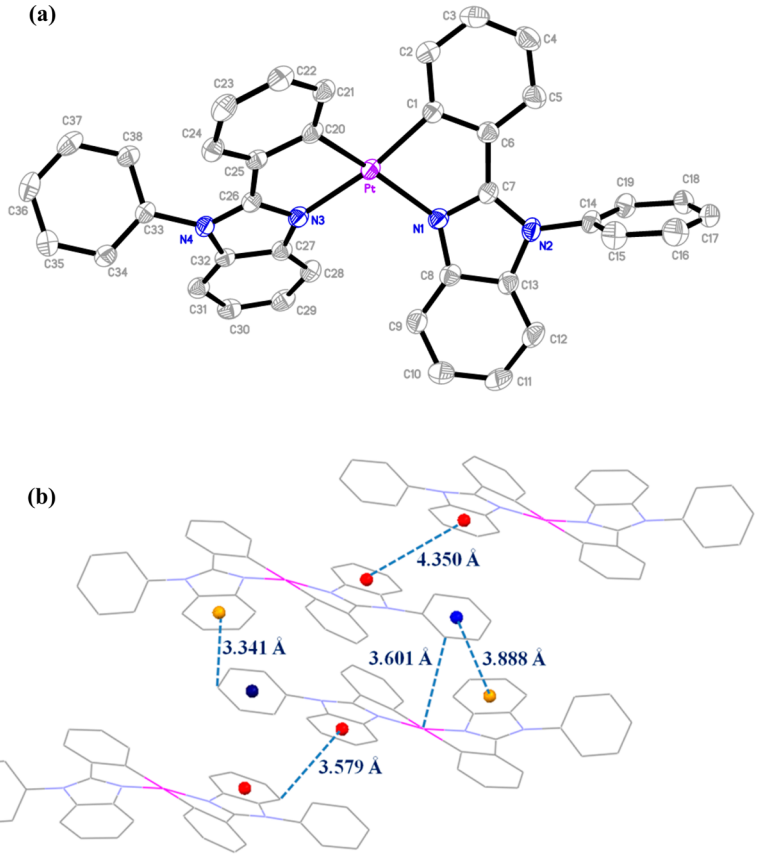

Figure 2. (a) Perspective view of complex $[Pt(PBI)_2]$ with thermal ellipsoids shown at the 30% probability level limit. Bond distances (Å): Pt−C(1) = 1.966(4), Pt−C(20) = 2.006(4), Pt−N(1) = 2.121(3), Pt−N(3) = 2.111(3). Bond angles (deg): C(1)−Pt−C(20) = 100.14(1), N(1)−Pt−N(3) = 105.13(4), C(20)−Pt−N(3) = 79.55(2), N(1)−Pt−C(1) = 79.86(2), C(1)−Pt−N(3) = 166.93(1), C(20)−Pt−N(1) = 159.13(2); (b) Crystal packing diagram of $[Pt(PBI)_2]$ (hydrogen atoms have been omitted for clarity).

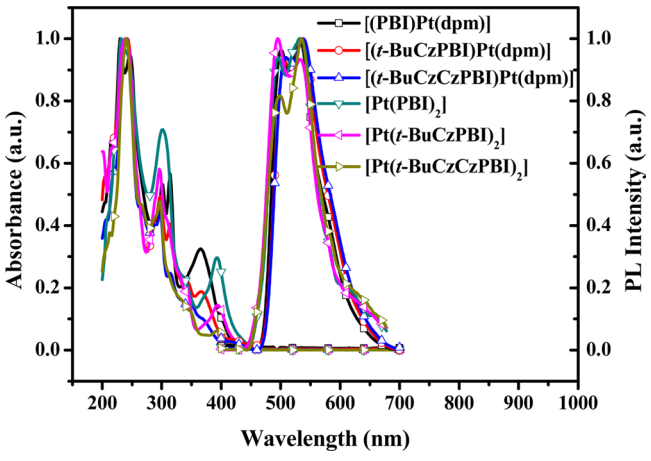

Figure 3. Normalized absorption and PL spectra of Pt(II) complexes in DCM solution at 10^{-5} M (PL spectra of the $[Pt(C^N)_2]$ complexes at 10^{-3} M).

[(PBI)Pt(acac)] has ideal square-planar configuration, while $[Pt(PBI)_2]$ displays antitwist square-planar fashion and nearly becomes quasi-tetrahedron either in ground state or in excited state (Table 2). This variation in geometry leads to two consequences according to the ligand field theory: (1) the d−d* energy splitting is reduced from the square-planar configuration of complex [(PBI)Pt(acac)] to the quasi-tetrahedron configuration of $[Pt(PBI)_2]$. The d−d* excited state of complex $[Pt(PBI)_2]$ may approach the energy minimum, which is an unfavorable state for luminescence because nonradiative deactivation have more accessible channels. As a result, the nonradiative rate constant (k_{nr}) of complex $[Pt(PBI)_2]$ (17.34×10^5 s^{-1}) is larger than that of [(PBI)Pt(acac)] (3.00×10^5 s^{-1}).[56] Likewise, as shown in Table 1, the complexes $[Pt(C^N)_2]$ have much greater k_{nr} ($>10^6$ s^{-1}) with the increasing of dendrons. (2) The energy differences between d_1 and other occupied d orbitals d_2, d_3, or d_4 are distinctly larger, so the energy denominations which govern the mixing between the MLCT states become greater in the distorted square-planar (quasi-tetrahedron) configuration than they do in the square-planar configuration; that is, the efficiency of SOC decreased or will not be attained. This leads to lower radiative rate constants (k_r) for the transitions from T_1 substates to the ground state S_0 ($[Pt(PBI)_2]$, 0.52×10^5 s^{-1}; [(PBI)Pt(acac)], 5.50×10^5 s^{-1}).[41] The different distribution diagrams of calculated energy levels for two complexes supported this speculation (Table 2). Thus, according to the equation $\varphi_p = k_r/(k_r + k_{nr})$, a smaller k_r and a larger k_{nr} for complex $[Pt(PBI)_2]$ would result in a smaller φ_p, and hence we could understand why these homoleptic Pt(II) complexes exhibit weaker emission at RT.

Electroluminescent Properties. Multilayer devices were fabricated with a configuration of indium tin oxide/poly(3,4-ethylenedioxythiophene):poly(styrenesulfonate) (ITO/PEDOT:PSS) (50 nm)/emissive layer (poly-(*N*-vinyl carbazole) (PVK):30% $[(C^N)Pt(dpm)]$ complexes) (30 nm)/2,7-bis-(diphenylphosphoryl)-9,9′-spirobi[fluorene] (SPPO13) (50

dx.doi.org/10.1021/ic402099x | *Inorg. Chem.* 2014, 53, 810−821

Table 2. Summary of MO Frontier Orbitals and Energy Levels Distribution Diagram of [(PBI)Pt(acac)] and [Pt(PBI)$_2$] by DFT Calculation

	[(PBI)Pt(acac)]	[Pt(PBI)$_2$]
Crystal structure	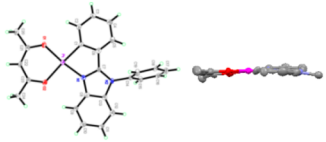	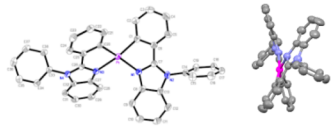
HOMO		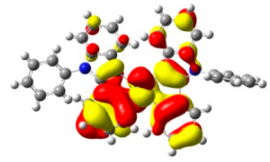
LUMO		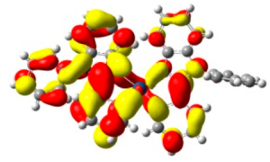
d% of HOMO	42.4	50.5
d% of LUMO	3.6	2.9
Ground state		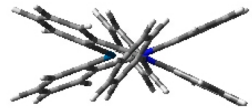
Excited state		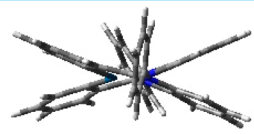
Energy levels distribution	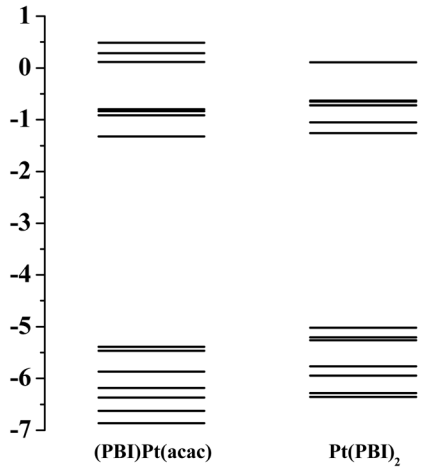	
Conclusion (RT)	Emitting	Weak Emitting

nm)/LiF (1 nm)/Al (100 nm) (device A) or ITO/PEDOT:PSS (50 nm)/emissive layer (4,4′-(*N*,*N*′-dicarbazole)-biphenyl (CBP):16% [Pt(C^N)$_2$] complexes) (30 nm)/2,9-dimethyl-4,7-diphenyl-1,10-phenanthroline (BCP) (15 nm)/tris(8-quinolinato)aluminium (Alq_3) (40 nm)/LiF (1 nm)/Al (100 nm) (device B) via a spin-coating process. For complexes [(C^N)Pt(dpm)], PVK was chosen as the host material and SPPO13 as the electron-transporting material due to the

dx.doi.org/10.1021/ic402099x | *Inorg. Chem.* 2014, 53, 810−821

obvious variation of HOMO and LUMO energy levels compared to the [(C^N)Pt(acac)] complexes (Table 1).[50] Molecular structures of PVK and SPPO13 are shown in Figure 4. The devices' performance characteristics are collected in

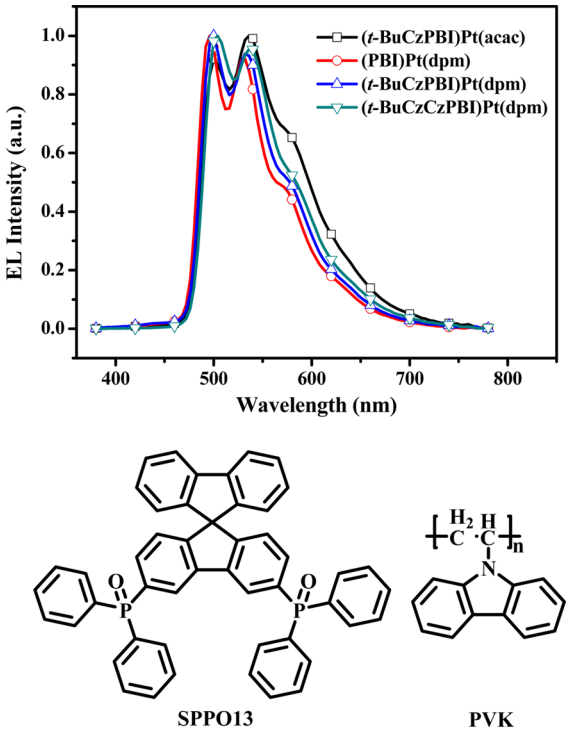

Figure 4. EL spectra of complexes [(C^N)Pt(dpm)] and [(*t*-BuCzPBI)Pt(acac)] at the driving voltage of 7 V, and the molecular structures of SPPO13 and PVK used in fabricating the EL devices.

Table 3. Analogously to the EL characterization results of complex [(*t*-BuCzPBI)Pt(acac)], using devices A and B indicates that the alteration of device structure has no obvious effect on the EL performance of complex [(*t*-BuCzPBI)Pt-(acac)]. So the data in Table 3 are comparable for complexes [(C^N)Pt(dpm)] and [(C^N)Pt(acac)] in spite of adopting a different device structure. The 30% doping concentration of complexes [(C^N)Pt(dpm)] was chosen to compare effectively the EL performance of these species with the [(*t*-BuCzPBI)-Pt(acac)] complex.

The turn-on voltage distinctly decreases going from complexes [(*t*-BuCzPBI)Pt(acac)], [(PBI)Pt(dpm)], and [(*t*-BuCzPBI)Pt(dpm)] to [(*t*-BuCzCzPBI)Pt(dpm)], owing to better solubility and high-quality film for the latter (Table 3). As shown in Figure 5a, the maximum brightness of device A is between 3437 and 7492 cd/m^2 and is lower than it is in previously reported devices (exceed 10000 cd/m^2). This should be attributed to the P═O group in the electron-transporting material SPPO13, which can significantly quench the luminescent brightness.[57] Figure 4 shows the EL spectra of [(C^N)Pt(dpm)] complexes at the driving voltage of 7 V. The devices exhibit a strong green emission at 496−538 nm, resembling the corresponding PL spectra in solution in spite of the relatively high doping concentration. Moreover, the shoulder peak at 577 nm of complexes [(C^N)Pt(dpm)] is obviously lower than that of complex [(*t*-BuCzPBI)Pt(acac)]. Such findings rule out any significant intermolecular interaction between the doping molecules in the device condition, which means bulky dpm ligand can effectively inhibit the

Table 3. EL Performance of the Devices

compound	V_{on} [a] (V)	B [b] (cd·m^{-2})	η_c [b] (cd·A^{-1})	η_p [b] (lm·W^{-1})	EQE [b] (%)	η_c [c] (cd·A^{-1})	η_p [c] (lm·W^{-1})	EQE [c] (%)	η_c [d] (cd·A^{-1})	η_p [d] (lm·W^{-1})	EQE [d] (%)	λ_{em} [b] (nm)	CIE (x, y)
[(*t*-BuCzPBI)Pt(acac)] [e]	6.0	13608	17.55	8.41	5.62	16.93	7.52	5.40	13.27	4.51	4.25	544	(0.39,0.56)
[(*t*-BuCzPBI)Pt(acac)] [f]	5.5	4007	16.18	6.83	5.09	14.53	6.46	4.53	11.66	3.91	3.65	500, 535	(0.32,0.56)
[(PBI)Pt(dpm)] [f]	4.3	3437	19.45	9.52	6.10	19.38	9.49	6.04	11.40	4.17	3.66	496, 531	(0.36,0.57)
[(*t*-BuCzPBI)Pt(dpm)] [f]	4.2	5412	24.76	15.99	7.77	24.60	12.22	7.70	19.40	8.34	6.09	499, 534	(0.30,0.56)
[(*t*-BuCzCzPBI)Pt(dpm)] [f]	3.5	7492	29.31	21.72	9.04	27.05	14.47	8.34	19.78	8.12	6.12	504, 538	(0.33,0.58)
[Pt(PBI)$_2$] [g]	10.0	344	0.34	0.07	0.10	0.14	0.04					560	(0.43,0.51)
[Pt(*t*-BuCzPBI)$_2$] [g]	6.0	1495	0.83	0.39	0.20	0.58	0.19		0.49	0.13		532	(0.38,0.53)
[Pt(*t*-BuCzCzPBI)$_2$] [g]	5.6	5021	2.71	1.68	0.74	1.73	0.70	0.57	1.62	0.55		520	(0.35,0.53)

[a] At a brightness of 1 cd·m^{-2}. [b] At the maximum. [c] At a brightness of 100 cd·m^{-2}. [d] At a brightness of 1000 cd·m^{-2}. [e] Reference 50. [f] Device A structure with 30 wt % dopant concentration and Commission Internationale de L'Eclairage (CIE) at 7 V. [g] Device B structure with 16 wt % dopant concentration and CIE at 14 V; V_{on}, turn on voltage; B, brightness; η_c current efficiency; η_p, power efficiency; EQE, external quantum efficiency.

dx.doi.org/10.1021/ic402099x | Inorg. Chem. 2014, 53, 810−821

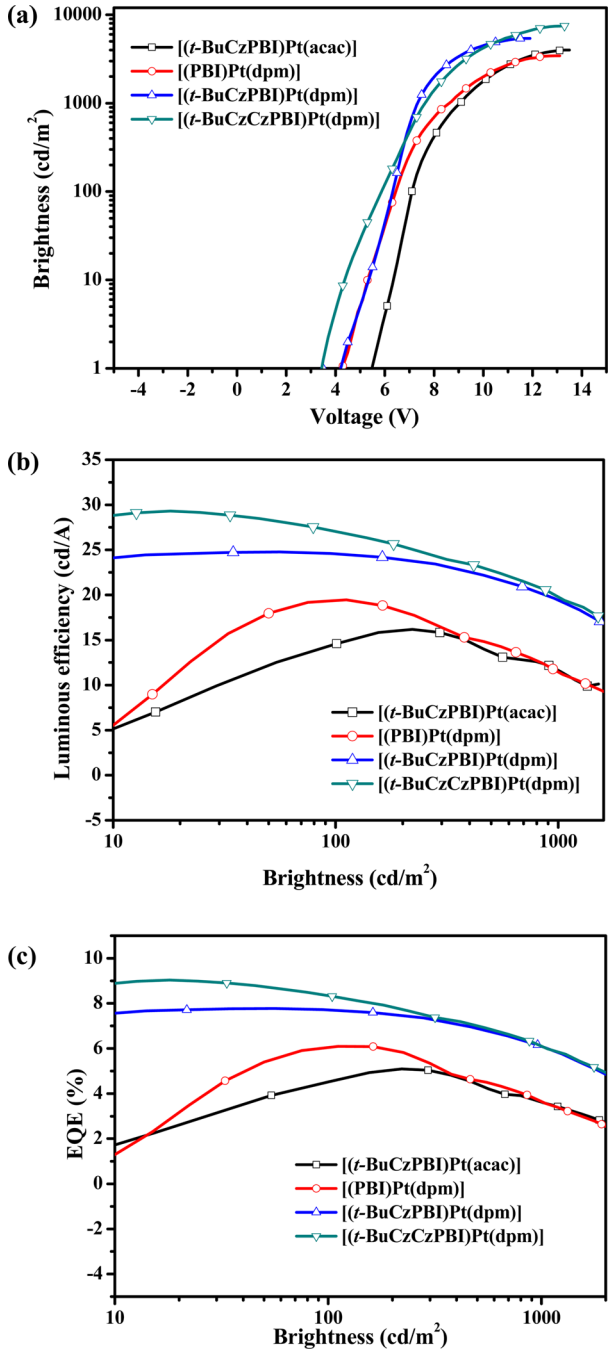

Figure 5. (a) Voltage–brightness, (b) brightness–CE, and (c) brightness–EQE characteristics of complexes [(C^N)Pt(dpm)] and [(*t*-BuCzPBI)Pt(acac)].

intermolecular interaction in the presence or absence of dendrons. It can be further verified by the brightness–efficiency characteristics of complexes [(C^N)Pt(dpm)]. As indicated in Figure 5b,c, the EL performance of complex [(*t*-BuCzPBI)Pt(dpm)] with peak CE of 24.76 cd/A, power efficiency of 15.99 lm/W, and EQE of 7.77% was achieved and enhanced by about 7 cd/A, 9 lm/W and 2%, respectively, compared with complex [(*t*-BuCzPBI)Pt(acac)], by simple alternation of ancillary ligand structure. The efficiency of nondendrimeric [(PBI)Pt(dpm)] (19.45 cd/A, 9.52 lm/W, and 6.10%) is also much higher than it is for dendrimeric [(*t*-BuCzPBI)Pt(acac)] (Table 3). In particular, dendrimeric molecular structure can further reduce the interaction between the emissive cores of Pt(II) complexes.[48−50] As shown in Figure 5, the luminescent efficiency at the same brightness increases when going from [(*t*-BuCzPBI)Pt(acac)], [(PBI)Pt(dpm)], and [(*t*-BuCzPBI)-Pt(dpm)] to [(*t*-BuCzCzPBI)Pt(dpm)]. As we expected, complex [(*t*-BuCzCzPBI)Pt(dpm)] gives the best performance, with a maximum CE of 29.31 cd/A, a maximum power efficiency of 21.72 lm/W, and a maximum EQE of 9.04% among the Pt(II) complexes, which is comparable to the reported efficient solution-processed OLEDs incorporating Pt(II)-based emitter.[58−60] In addition, these [(C^N)Pt(dpm)] complexes show a slow efficiency roll-off with increasing brightness or current density (Table 3). For example, at brightness of 100 cd/m^2 and 1000 cd/m^2, the CE of complex [(*t*-BuCzCzPBI)Pt(dpm)] remains 27.05 cd/A (EQE 8.34%) and 19.78 cd/A (EQE 6.12%) and only the decreases of 7.7% and 32.5% are observed, respectively.

OLEDs based on three homoleptic dendrimeric [Pt(C^N)$_2$] complexes doped into CBP at 16% by weight were fabricated and characterized in device B structure. On the basis of their solution behavior, at the outset we predicted that they would give rise to worse EL properties. The best performances were shown by complex [Pt(*t*-BuCzCzPBI)$_2$], with the maximum brightness of 5021 cd/m^2, CE of 2.71 cd/A, power efficiency of 1.68 lm/W, and EQE of 0.74% (Table 3). Such poor efficiency stems from the relatively low φ_p of the distorted emitting core; however, the data obtained from these devices display two notable features. As illustrated in Figure 6, a decreased red shift from 1674 to 262 cm^{-1} in EL spectra compared to PL spectra in solution (Tables 1 and 3) and an increased CE from 0.34 (EQE 0.10%) to 2.71 cd/A (EQE 0.74%) are observed in order of nondendrimeric [Pt(PBI)$_2$], dendrimeric [Pt(*t*-BuCzPBI)$_2$], and extended dendrimeric [Pt(*t*-BuCzCzPBI)$_2$] complexes. This is clearly attributed to the effect of dendrons on decreasing aggregation and triplet–triplet (T–T) annihilation processes in the solid. That is to say, dendrimeric homoleptic [Pt(C^N)$_2$] complexes have such ability to inhibit intermolecular interaction depending obviously on the size of the dendrons, which is benefit to improve the optoelectronic properties of Pt(II) complexes, as discussed before.

CONCLUSIONS

In this study, we reported the synthesis, structure, and optoelectronic investigation of a series of dendrimeric Pt(II) complexes, which were designed to avoid the formation of aggregates or excimers through incorporating bulky *t*-butyl group or adopting homoleptic configuration. Improved emission properties have been realized, including increased φ_p, hardly changed EL spectra, enhanced EL efficiency, and slow efficiency roll-off. The complex [(*t*-BuCzCzPBI)Pt(dpm)] showed the best performance, with a peak CE of 29.31 cd/A (EQE 9.04%) in solution-processed OLED incorporating Pt(II)-based dendrimers so far. Homoleptic dendrimeric complexes [Pt(C^N)$_2$] should be more effective for suppressing the intermolecular interaction relative to heteroleptic [(C^N)Pt(acac)] species. However, they exhibited poor luminescent behavior due to severely distorted square-planar geometry of the emitting core, which had been clarified by X-ray single diffraction analysis and DFT calculations. Nevertheless, the powder φ_p and the EL performance of dendrimeric emitter are still far superior to those of a nondendrimeric one, because of the encapsulation and isolation effect of dendrons. Such molecular design strategy would be successful and

dx.doi.org/10.1021/ic402099x | *Inorg. Chem.* 2014, 53, 810−821

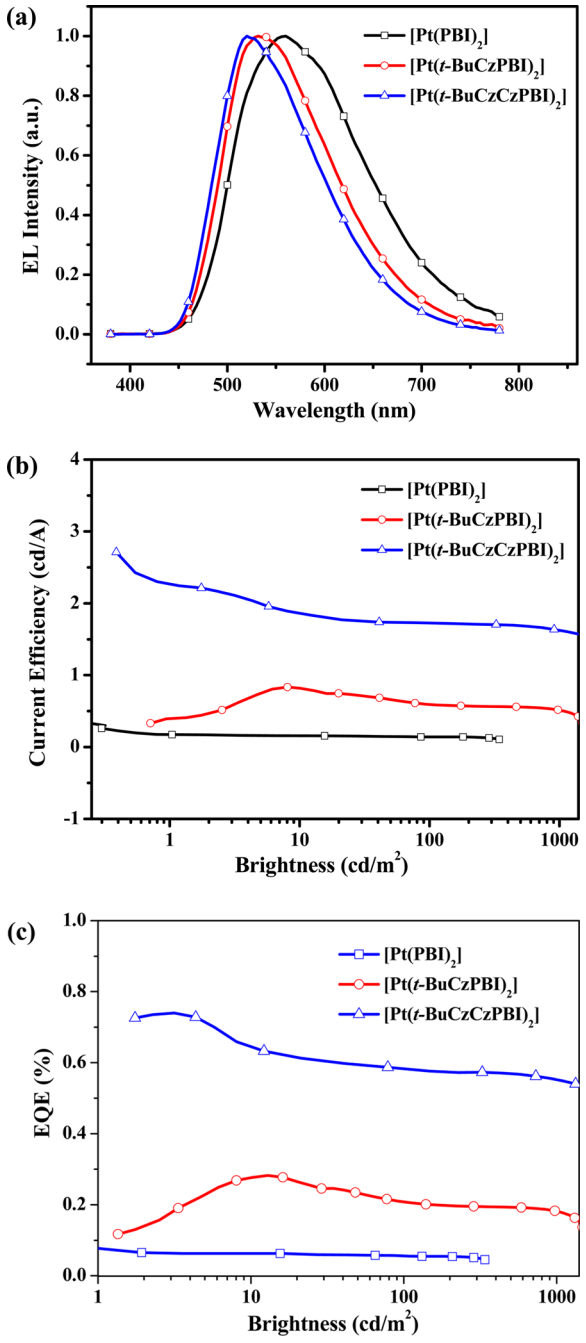

Figure 6. (a) EL spectra at the driving voltage of 14 V. (b) Brightness−CE and (c) brightness−EQE characteristics of [Pt-(C^N)$_2$] complexes.

promising for developing the highly efficient Pt(II) complexes emitting materials, once the Pt(II) complex core has perfect square-planar geometry.

EXPERIMENTAL SECTION

Methods and Materials. All reactions and manipulations were carried out under argon atmosphere. All chemicals and reagents (analytical reagent grade) for chemical synthesis were used as received from commercial sources. Some solvents, such as DCM, THF, toluene, and chlorobenzene were distilled carefully by standard procedures prior to use. The ^{1}H and ^{13}C NMR spectra were recorded on Bruker Avance 300/600 MHz NMR spectrometer. Elemental analyses were carried out using a Bio-Rad Company elemental analytical instrument. The MALDI-TOF mass spectra were obtained on an Autoflex III TOF apparatus. The TGA was performed under a flow of nitrogen at a heating rate of 10 °C/min with a Perkin-Elmer TGA 7 thermal gravimetric analyzer. The experimental error is estimated to be ±10%. Ultraviolet−visible (UV−vis) absorption and PL spectra were measured on a Perkin-Elmer Lambda 35 UV−vis spectrometer and a Perkin-Elmer LS 50B spectrofluorometer in aerated solution, respectively. Cyclic voltammetry experiments were performed with an EG&G 283 (Princeton Applied Research) potentiostat/galvanostat system at RT with a conventional three-electrode system consisting of a Pt working electrode, a Pt counter electrode, and a Ag/AgCl reference electrode. The supporting electrolyte was 0.1 M tetrabutylammonium perchlorate (n-Bu$_4$NClO$_4$). The potentials are quoted against the ferrocene standard. The lifetime of the samples was obtained by an exponential fit of emission decay curves recorded with the laser photolysis technique, in which the third harmonic of a neodymium-doped yttrium aluminum garnet laser (355 nm output and ca. ∼3 ns pulse width) was used as the excitation source, coupled with a fast-response photomultiplier. The solution PL quantum efficiencies were measured and calculated by a relative method using [(ppy)Pt(acac)] (Φ_{em} = 0.15) as a reference.[5] The powder and film PL quantum efficiency was determined with an integrating sphere under a 409 nm excitation wavelength of a He−Cd laser. The ligands 1,2-diphenylbenzoimidazole (H-PBI), 1-phenyl-2-(2-bromophenyl)-benzoimidazole (Br-PBI), 1-(4-(3,6-di-t-butylcarbazol-9-yl))phenyl-2-phenylbenzoimidazole (*t*-BuCz-H-PBI), 1-(4-(3,6-di-t-butylcarbazol-9-yl))phenyl-2-(2-bromophenyl)benzoimidazole (*t*-BuCz-Br-PBI), 1-(4-(3,6-di-(3,6 -di-t-butyl-carbazol-9-yl))carbazol-9-yl)phenyl-2-phenyl-benzoimidazole (*t*-BuCzCz-H-PBI) and 1-(4-(3,6-di-(3,6-di-t-butyl-carbazol-9-yl))carbazol-9-yl)phenyl-2-(2 -bromophenyl)-benzoimidazole (*t*-BuCzCz-Br-PBI) were prepared according to the literature procedures.[48,50] *trans*-Pt(SEt$_2$)$_2$Cl$_2$ was prepared according to the procedure given by Kaufmann et al.[61] The syntheses, characterization, and optoelectronic properties of the [(PBI)Pt(acac)] and [(*t*-BuCzPBI)Pt(acac)] complexes were previously reported by our group.[51]

Preparation of Pt(II) Complexes. General procedures for the construction of heteroleptic Pt(II) complexes: A mixture of K$_2$PtCl$_4$ and H−C^N-chelate ligand (H-PBI, *t*-BuCz-H-PBI, *t*-BuCzCz-H-PBI) (2.05 equiv.) in 2-ethoxyethanol and H$_2$O (3:1 v/v) was stirred at 60 °C for 24, 48, and 72 h, respectively. After it was cooled to RT, the solvent was removed by reduced pressure distillation, and the vacuum-dried green-yellow chloro-bridged dimer was obtained. Then, the dimer was suspended in 2-ethoxyethanol and reacted with dipivaloylmethane (Hdpm) (3 equiv) and anhydrous Na$_2$CO$_3$ (3 equiv) at 80 °C for 24, 48, and 72 h, respectively. The resulting mixture was poured into water and extracted with DCM. The combined organic layers were washed with water and dried over anhydrous sodium sulfate. After the volatiles were completely removed under reduced pressure, the residue was purified by column chromatography on silica gel using DCM/petroleum (PE) (1:2 v/v) as the eluent to afford pure product.

[(PBI)Pt(dpm)]. Yield: 21.2%. ^{1}H NMR (300 MHz, CDCl$_3$, ppm): δ 8.67 (d, J = 8.1 Hz, 1H), 7.78 (d, J = 7.2 Hz, 1H), 7.69−7.67 (m, 3H), 7.53−7.49 (m, 2H), 7.38 (td, J = 8.0, 0.9 Hz, 1H), 7.25 (td, J = 8.1, 0.9 Hz, 1H), 7.10 (td, J = 7.5, 1.2 Hz, 1H), 7.03 (d, J = 7.8 Hz, 1H), 6.75 (t, J = 7.5 Hz, 1H), 6.45 (d, J = 7.5 Hz, 1H), 5.89 (s, 1H), 1.37 (s, 9H), 1.31 (s, 9H). ^{13}C NMR (151 MHz, CDCl$_3$, ppm): δ 193.7, 191.8, 162.5, 138.9, 138.5, 134.6, 133.8, 133.3, 129.9, 129.3, 129.2, 128.2, 127.0, 123.0, 122.9, 121.6, 115.8, 109.3, 91.9, 41.1, 40.0, 27.7, 27.6. Anal. Calcd for C$_{30}$H$_{32}$N$_2$O$_2$Pt: C, 55.63; H, 4.98; N, 4.33. Found: C, 55.29; H, 5.13; N, 3.96%. MALDI-TOF (m/z): 648.2 [M+H]$^+$.

[(t-BuCzPBI)Pt(dpm)]. Yield: 27.0%. ^{1}H NMR (300 MHz, CDCl$_3$, ppm): δ 8.72 (d, J = 8.1 Hz, 1H), 8.19 (s, 2H), 7.90 (d, J = 8.7 Hz, 2H), 7.82 (d, J = 7.5 Hz, 1H), 7.74 (d, J = 8.4 Hz, 2H), 7.55 (s, 4H), 7.42 (t, J = 7.4 Hz, 1H), 7.33 (t, J = 7.4 Hz, 1H), 7.20 (d, J = 8.4 Hz, 1H), 7.16 (t, J = 7.2 Hz, 1H), 6.85 (t, J = 7.5 Hz, 1H), 6.64 (d, J = 7.8 Hz, 1H), 5.91 (s, 1H), 1.50 (s, 18H), 1.38 (s, 9H), 1.32 (s, 9H). ^{13}C NMR (151 MHz, CDCl$_3$, ppm): δ 193.8, 191.9, 162.7, 142.7, 139.1, 139.0, 138.7, 137.6, 134.6, 133.2, 131.6, 130.1, 128.5, 128.4, 126.8, 123.3, 122.9, 122.86, 122.8, 122.5, 121.8, 116.0, 115.5, 109.3, 108.0, 92.0, 41.2, 40.0, 33.7, 30.9, 27.7, 27.6. Anal. Calcd for C$_{50}$H$_{55}$N$_3$O$_2$Pt:

dx.doi.org/10.1021/ic402099x | Inorg. Chem. 2014, 53, 810−821

C, 64.92; H, 5.99; N, 4.54. Found: C, 64.63; H, 6.08; N, 4.22%. MALDI-TOF (m/z): 925.4 $[M+H]^+$.

[(t-BuCzCzPBI)Pt(dpm)]. Yield: 39.0%. ^{1}H NMR (300 MHz, $CDCl_3$, ppm): δ 8.75 (d, J = 8.1 Hz, 1H), 8.30 (d, J = 2.1 Hz, 2H), 8.18 (d, J = 1.8 Hz, 4H), 8.11 (d, J = 8.7 Hz, 2H), 7.90 (d, J = 8.7 Hz, 2H), 7.86−7.82 (m, 3H), 7.72 (dd, J = 8.7, 2.1 Hz, 2H), 7.50−7.36 (m, 10H), 7.25 (d, J = 7.5 Hz, 1H), 7.18 (td, J = 7.4, 1.2 Hz, 1H), 6.91 (td, J = 7.5, 0.9 Hz, 1H), 6.72 (dd, J = 7.8, 0.6 Hz, 1H), 5.92 (s, 1H), 1.48 (s, 36H), 1.39 (s, 9H), 1.33 (s, 9H). ^{13}C NMR (151 MHz, $CDCl_3$, ppm): δ 193.8, 192.0, 162.7, 141.7, 139.1, 139.0, 138.7, 138.1, 134.5, 132.9, 130.6, 130.2, 129.0, 128.5, 127.6, 125.2, 123.5, 123.4, 122.7, 122.6, 122.5, 122.1, 121.8, 118.5, 116.1, 115.2, 109.9, 109.2, 108.0, 92.0, 41.2, 40.0, 33.7, 31.0, 27.7, 27.6. Anal. Calcd for $C_{82}H_{85}N_5O_2Pt$: C, 72.01; H, 6.26; N, 5.12. Found: C, 71.87; H, 6.35; N, 4.96%. MALDI-TOF (m/z): 1367.6 $[M+H]^+$.

General procedures for the synthesis of homoleptic Pt(II) complexes: To a stirred solution of Br−C^N-chelate ligand (Br-PBI, *t*-BuCz-Br-PBI, *t*-BuCzCz-Br-PBI) (2.1 equiv) in anhydrous THF was slowly added *n*-butyllithium (2.2 equiv, 2.5 M in hexane) at −78 °C. After it was stirred for 45 min, a solution of *trans*-$Pt(SEt_2)_2Cl_2$ in anhydrous THF was added dropwise to the reaction mixture. The resulting mixture was stirred continuously for 30 min at −78 °C; then the temperature was allowed to rise slowly to RT. The reaction mixture was hydrolyzed with methanol. The volatiles were removed under reduced pressure, and the residue was recrystallized from diethyl ether and ethanol, respectively. If the precipitate was still impure, further purification by flash chromatography (alkaline Al_2O_3 filler, PE/diethyl ether = 3:2 v/v) was carried out.

[Pt(PBI)$_2$]. Yield: 56.5%. ^{1}H NMR (300 MHz, $CDCl_3$, ppm): δ 8.25 (d, J = 8.1 Hz, 1H), 7.89 (dd, J = 7.1, 1.8 Hz, 1H), 7.72−7.68 (m, 3H), 7.59−7.56 (m, 3H), 7.23 (td, J = 6.8, 1.5 Hz, 1H), 7.18 (td, J = 7.2, 1.2 Hz, 1H), 7.09 (dd, J = 10.0, 1.8 Hz, 1H), 6.82 (t, J = 7.2 Hz, 1H), 6.66 (dd, J = 7.7, 1.2 Hz, 1H). ^{13}C NMR (75 MHz, $CDCl_3$): δ 164.5, 150.3, 141.2, 138.1, 137.9, 136.2, 135.8, 131.3, 130.8, 130.5, 128.7, 125.4, 123.7, 123.5, 122.5, 119.4, 110.9. Anal.Calcd for $C_{38}H_{26}N_4Pt$: C, 62.20; H, 3.57; N, 7.64. Found: C, 62.57; H, 3.34; N, 7.26%. MALDI-TOF(m/z): 733.1 $[M+H]^+$.

[Pt(t-BuCzPBI)$_2$]. Yield: 48.6%. ^{1}H NMR (300 MHz, $CDCl_3$, ppm): δ 8.32 (d, J = 8.4 Hz, 1H), 8.20 (s, 2H), 7.98 (d, J = 8.4 Hz, 1H), 7.93 (d, J = 8.7 Hz, 2H), 7.81 (d, J = 8.7 Hz, 2H), 7.57 (d, J = 1.2 Hz, 4H), 7.35−7.23 (m, 4H), 6.95 (t, J = 7.5 Hz, 1H), 6.86 (dd, J = 9.0, 1.2 Hz, 1H), 1.51 (s, 18H). ^{13}C NMR (75 MHz, $CDCl_3$): δ 164.7, 150.4, 144.2, 141.9, 141.2, 140.4, 139.1, 138.1, 135.7, 134.1, 131.0, 130.1, 128.4, 125.4, 124.4, 124.3, 124.0, 123.8, 122.8, 119.6, 116.9, 110.9, 109.6, 35.2, 32.4. Anal. Calcd for $C_{78}H_{72}N_6Pt$: C, 72.71; H, 5.63; N, 6.52. Found: C, 72.42; H, 5.85; N, 6.59%. MALDI-TOF(m/z): 1288.7 $[M+H]^+$.

[Pt(t-BuCzCzPBI)$_2$]. Yield: 32.0%. ^{1}H NMR (300 MHz, $CDCl_3$, ppm): δ 8.35 (d, J = 8.4 Hz, 1H), 8.30 (d, J = 1.8 Hz, 2H), 8.18 (d, J = 1.5 Hz, 4H), 8.13 (d, J = 8.7 Hz, 2H), 8.02 (d, J = 8.4 Hz, 1H), 7.98 (d, J = 8.7 Hz, 2H), 7.86 (d, J = 8.7 Hz, 2H), 7.74 (dd, J = 8.7, 1.8 Hz, 2H), 7.49 (dd, J = 8.7, 1.8 Hz, 4H), 7.40−7.29 (m, 8H), 7.01 (t, J = 7.5 Hz, 1H), 6.94 (d, J = 6.9 Hz, 1H), 1.48 (s, 36H). ^{13}C NMR (75 MHz, $CDCl_3$): δ 164.8, 150.4, 143.1, 141.4, 140.5, 140.4, 139.4, 138.0, 135.6, 135.4, 132.1, 131.2, 130.7, 129.2, 126.7, 124.9, 124.0, 123.6, 122.8, 120.0, 116.7, 111.4, 109.5, 35.2, 32.5. Anal. Calcd for $C_{142}H_{132}N_{10}Pt$: C, 78.46; H, 6.12; N, 6.44. Found: C, 78.53; H, 6.12; N, 6.71%. MALDI-TOF(m/z): 2173.1 $[M+H]^+$.

Crystal Structure Determination. Crystals of complexes [(PBI)-Pt(acac)] and $[Pt(PBI)_2]$ were obtained by slow evaporation of DCM/MeOH solution at RT. The crystal data and details of data collection and refinement were summarized in Supporting Information, Table S3. The single-crystal X-ray diffraction experiments were carried out using a Bruker Smart APEX diffractometer with CCD detector and graphite monochromator, Mo Kα radiation (λ = 0.71073 Å). The intensity data were recorded with ω scan mode (187 K). Lorentz polarization factors were made for the intensity data, and absorption corrections were performed using SADABS program.[62] The crystal structure was determined using the SHELXTL program and refined using full matrix least-squares.[63] All non-hydrogen atoms were assigned with anisotropic displacement parameters, whereas hydrogen atoms were placed at calculated theoretical positions and included in the final cycles of refinement in a riding model along with attached carbons.

DFT Calculations. All calculations have been performed on an Origin/3900 server, using the Gaussian 03 program package.[64] The ground-state structures were optimized by the DFT using the B3PW91 hybrid functional. The "double-ξ" basis set LANL2DZ,[65−67] consisting of 18 valence electrons associated with the pseudopotential, was employed for Pt atom and 6-31G(d) basis sets for H, C, O and N atoms. Following each ground state optimization, the vibrational frequencies were calculated, and the results showed that all optimized structures were stable geometric structures. The calculated electronic density plots for HOMO and LUMO orbitals were prepared using GaussView 4.1.2 software. In addition, compositions of molecular orbitals and overlap populations between molecular fragments were analyzed using the PYMOLYZE program.[68]

OLED Fabrication and Measurements. The OLEDs were fabricated with a structure of ITO/PEDOT:PSS (50 nm)/emissive layer (PVK:30% [(C^N)Pt(dpm)] complexes) (30 nm)/SPPO13 (50 nm)/LiF (1 nm)/Al (100 nm) (device A) or ITO/PEDOT:PSS (50 nm)/emissive layer (CBP:16% $[Pt(C^N)_2]$ complexes) (30 nm)/BCP (15 nm)/Alq_3 (40 nm)/LiF (1 nm)/Al (100 nm) (device B). The PEDOT:PSS and emissive layers (chlorobenzene was used as the solvent) were spin-coated in sequence onto the precleaned and UV−ozone-treated ITO substrate, respectively, followed by thermal evaporation of the SPPO13 (50 nm)/ or BCP (15 nm)/Alq_3 (40 nm)/, LiF (1 nm)/Al (100 nm) structure in vacuum chamber at a base pressure of less than 4×10^{-4} Pa. The current-density−voltage and brightness−voltage curves of the devices were measured using a Keithley 2400 source meter with a calibrated silicon photodiode. The EL spectra and CIE coordinates were recorded using the PR650 spectra colorimeter. All the experiments and measurements were carried out at RT under ambient conditions.

■ ASSOCIATED CONTENT

Supporting Information

X-ray crystallographic data for [(PBI)Pt(acac)] and $[Pt(PBI)_2]$ in CIF format; crystal data and structure refinement details; additional photophysical data and spectra. This material is available free of charge via the Internet at http://pubs.acs.org.

■ AUTHOR INFORMATION

Corresponding Author

*E-mail: hmzhan@ciac.jl.cn.

Notes

The authors declare no competing financial interest.

■ ACKNOWLEDGMENTS

The work was financially supported by the National Natural Science Foundation of China (No. 51073152 and 21204083) and 973 Project (No. 2009CB623600).

■ REFERENCES

(1) Baldo, M. A.; O'Brien, D. F.; You, Y.; Shoustikov, A.; Sibley, S.; Thompson, M. E.; Forrest, S. R. *Nature* **1998**, *347*, 151−154.
(2) Chi, Y.; Chou, P.-T. *Chem. Soc. Rev.* **2010**, *39*, 638−655.
(3) Kalinowski, J.; Fattori, V.; Cocchi, M.; Williams, J. A. G. *Coord. Chem. Rev.* **2011**, *255*, 2401−2425.
(4) Williams, J. A. G. *Chem. Soc. Rev.* **2009**, *38*, 1783−1801.
(5) Brooks, J.; Babayan, Y.; Lamansky, S.; Djurovich, P. I.; Irina, T.; Bau, R.; Thompson, M. E. *Inorg. Chem.* **2002**, *41*, 3055−3066.
(6) D'Andrade, B. W.; Forres, S. R. *J. Appl. Phys.* **2003**, *94*, 3101−3109.
(7) Ma, B.; Djurovich, P. I.; Garon, S.; Alleyne, B.; Thompson, M. E. *Adv. Funct. Mater.* **2006**, *16*, 2438−2446.

(8) Chang, S.-Y.; Chen, J.-L.; Chi, Y. *Inorg. Chem.* **2007**, *46*, 11202−11212.
(9) Yang, X.; Wang, Z.; Madakuni, S.; Li, J.; Jabbour, G. E. *Adv. Mater.* **2008**, *20*, 2405−2409.
(10) Unger, Y.; Meyer, D.; Molt, O.; Schildknecht, C.; Münster, I.; Wagenblast, G.; Strassner, T. *Angew. Chem., Int. Ed.* **2010**, *49*, 10214−10216.
(11) Hang, X.-C.; Fleetham, T.; Turner, E.; Brooks, J.; Li, J. *Angew. Chem., Int. Ed.* **2013**, *52*, 6753−6756.
(12) Turner, E.; Bakken, N.; Li, J. *Inorg. Chem.* **2013**, *52*, 7344−7351.
(13) Sotoyama, W.; Satoh, T.; Sawatari, N.; Inoue, H. *Appl. Phys. Lett.* **2005**, *86*, 153505.
(14) Wong, W.-Y.; He, Z.; So, S.-K.; Tong, K.-L.; Lin, Z. *Organometallics* **2005**, *24*, 4079−4082.
(15) Yang, C.; Zhang, X.; You, H.; Zhu, L.; Chen, L.; Zhu, L.; Tao, Y.; Ma, D.; Shuai, Z.; Qin, J. *Adv. Funct. Mater.* **2007**, *17*, 651−661.
(16) Zhou, G.-J.; Wong, W.-Y.; Yao, B.; Xie, Z.; Wang, L. *J. Mater. Chem.* **2008**, *18*, 1799−1809.
(17) Cocchi, M.; Virgili, D.; Fattori, V.; Rochester, D. L.; Williams, J. A. G. *Adv. Funct. Mater.* **2007**, *17*, 285−289.
(18) Yang, X.; Froehlich, J. D.; Chae, H. S.; Harding, B. T.; Li, S.; Mochizuki, A.; Jabbour, G. E. *Chem. Mater.* **2010**, *22*, 4776−4782.
(19) Kwong, R. C.; Sibley, S.; Dubovoy, T.; Baldo, M.; Forrest, S. R.; Thompson, M. E. *Chem. Mater.* **1999**, *11*, 3709−3713.
(20) Lin, Y.-Y.; Chan, S.-C.; Chan, M. C. W.; Hou, Y.-J.; Zhu, N.; Che, C.-M.; Liu, Y.; Wang, Y. *Eur. J. Inorg. Chem.* **2003**, *9*, 1263−1272.
(21) Che, C.-M.; Chan, S.-C.; Xiang, H.-F.; Chan, M. C. W.; Liu, Y.; Wang, Y. *Chem. Commum.* **2004**, 1484−1485.
(22) Lu, W.; Mi, B.-X.; Chan, M. C. W.; Hui, Z.; Che, C.-M.; Zhu, N.; Lee, S.-T. *J. Am. Chem. Soc.* **2004**, *126*, 4958−4971.
(23) Ikai, M.; Ishikawa, F.; Aratani, N.; Osuka, A.; Kawabata, S.; Kajioka, T.; Takeuchi, H.; Fujikawa, H.; Taga, Y. *Adv. Funct. Mater.* **2006**, *16*, 515−519.
(24) Yuen, M.-Y.; Kui, S. C. F.; Low, K.-H.; Kwok, C.-C.; Chui, S. S.-Y.; Ma, C.-W.; Zhu, N.; Che, C.-M. *Chem.—Eur. J.* **2010**, *16*, 14131−14141.
(25) Velusamy, M.; Chen, C.-H.; Wen, Y. S.; Lin, J. T.; Lin, C.-C.; Lai, C.-H.; Chou, P.-T. *Organometallics* **2010**, *29*, 3912−3921.
(26) Sun, W. F.; Zhang, B. G.; Li, Y. J.; Pritchett, T. M.; Li, Z. J.; Haley, J. E. *Chem. Mater.* **2010**, *22*, 6384−6392.
(27) Sommer, J. R.; Shelton, A. H.; Parthasarathy, A.; Ghiviriga, I.; Reynolds, J. R.; Schanze, K. S. *Chem. Mater.* **2011**, *23*, 5296−5304.
(28) Graham, K. R.; Yang, Y.; Sommer, J. R.; Shelton, A. H.; Schanze, K. S.; Xue, J.; Reynolds, J. R. *Chem. Mater.* **2011**, *23*, 5305−5312.
(29) Adamovich, V.; Brooks, J.; Tamayo, A.; Alexander, A. M.; Djurovich, P. I.; D'Andrade, B. W.; Adachi, C.; Forrest, S. R.; Thompson, M. E. *New J. Chem.* **2002**, *26*, 1171−1178.
(30) He, Z.; Wong, W.-Y.; Yu, X.; Kwok, H.-S.; Lin, Z. *Inorg. Chem.* **2006**, *45*, 10922−10937.
(31) Zhou, G. J.; Wang, Q.; Wang, X. Z.; Ho, C. L.; Wong, W. Y.; Ma, D. G.; Wang, L. X.; Lin, Z. Y. *J. Mater. Chem.* **2010**, *20*, 7472−7484.
(32) Mroz, W.; Botta, C.; Giovanella, U.; Rossi, E.; Colombo, A.; Dragonetti, C.; Roberto, D.; Ugo, R.; Valore, A.; Williams, J. A. G. *J. Mater. Chem.* **2011**, *21*, 8653−8661.
(33) Williams, J. A. G. *Top. Curr. Chem.* **2007**, *281*, 205−268.
(34) Ma, B.; Li, J.; Djurovich, P. I.; Yousufuddin, M.; Bau, R.; Thompson, M. E. *J. Am. Chem. Soc.* **2005**, *127*, 28−29.
(35) Kui, S. C. F.; Chow, P. K.; Tong, G. S. M.; Lai, S.-L.; Cheng, G.; Kwok, C.-C.; Low, K.-H.; Ko, M. Y.; Che, C.-M. *Chem.—Eur. J.* **2013**, *19*, 69−73.
(36) Murphy, L.; Brulatti, P.; Fattori, V.; Cocchi, M.; Williams, J. A. G. *Chem. Commun.* **2012**, *48*, 5817−5819.
(37) Fleetham, T.; Wang, Z.; Li, J. *Org. Electron.* **2012**, *13*, 1430−1345.
(38) Fleetham, T.; Ecton, J.; Wang, Z.; Bakken, N.; Li, J. *Adv. Mater.* **2013**, *25*, 2573−2576.
(39) Pettijohn, C. N.; Jochnowitz, E. B.; Chuong, B.; Nagle, J. K.; Vogler, A. *Coord. Chem. Rev.* **1998**, *171*, 85−92.
(40) Ma, B.; Djurovich, P. I.; Thompson, M. E. *Coord. Chem. Rev.* **2005**, *249*, 1501−1510.
(41) Yersin, H.; Rausch, A. F.; Czerwieniec, R.; Hofbeck, T.; Fischer, T. *Coord. Chem. Rev.* **2011**, *255*, 2622−2652.
(42) Mydlak, M.; Mauro, M.; Polo, F.; Felicetti, M.; Leonhardt, J.; Diener, G.; Cola, L. D.; Strassert, C. A. *Chem. Mater.* **2011**, *23*, 3659−3667.
(43) Kavitha, J.; Chang, S. Y.; Chi, Y.; Yu, J. K.; Hu, Y. H.; Chou, P. T.; Peng, S. M.; Lee, G. H.; Tao, Y. T.; Chien, C. H.; Carty, A. J. *Adv. Funct. Mater.* **2005**, *15*, 223−229.
(44) Cocchi, M.; Fattori, V.; Virgili, D.; Sabatini, C.; Marco, P. D. *Appl. Phys. Lett.* **2004**, *84*, 1052−1054.
(45) Chang, S.-Y.; Kavitha, J.; Li, S.-W.; Hsu, C.-S.; Chi, Y.; Yeh, Y.-S.; Chou, P.-T.; Lee, G.-H.; Carty, A. J.; Tao, Y.-T.; Chien, C.-H. *Inorg. Chem.* **2006**, *45*, 137−146.
(46) Hecht, S.; Freche, J. M. J. *Angew. Chem., Int. Ed.* **2001**, *40*, 74−91.
(47) Markham, J. P. J.; Magennis, S. W.; Burn, P. L.; Salata, O. V.; Samuel, I. D. W. *Adv. Mater.* **2002**, *14*, 975−979.
(48) Ding, J.; Gao, J.; Cheng, Y.; Xie, Z.; Wang, L.; Ma, D.; Jing, X.; Wang, F. *Adv. Funct. Mater.* **2006**, *16*, 575−581.
(49) Ding, J.; Lu, J.; Cheng, Y.; Xie, Z.; Wang, L.; Jing, X.; Wang, F. *Adv. Funct. Mater.* **2008**, *18*, 2754−2762.
(50) Li, H.; Ding, J.; Xie, Z.; Cheng, Y.; Wang, L. *J. Organomet. Chem.* **2009**, *694*, 2777−2785.
(51) Rillema, D. P.; Cruz, A. J.; Moore, C.; Siam, K.; Jehan, A.; Base, D.; Nguyen, T.; Huang, W. *Inorg. Chem.* **2013**, *52*, 596−607.
(52) Chassot, L.; Zelewsky, A. V.; Sandrini, D.; Maestri, M.; Balzan, V. *J. Am. Chem. Soc.* **1986**, *108*, 6084−6085.
(53) Chassot, L.; Zelewsky, A. V. *Inorg. Chem.* **1987**, *26*, 2814−2818.
(54) Jolliet, P.; Gianini, M.; Zelewsky, A.; Bernardinelli, G.; Stoeckli-Evans, H. *Inorg. Chem.* **1996**, *35*, 4883−4888.
(55) Li, H.; Yuan, W.; Wang, X.; Chen, B.; Cheng, Y.; Xie, Z.; Wang, L. *Chinese J. Appl. Chem.* **2012**, 1148−1157.
(56) Tong, G. S.-M.; Che, C.-M. *Chem.—Eur. J.* **2009**, *15*, 7225−7237.
(57) Shao, S.; Ding, J.; Ye, T.; Xie, Z.; Wang, L.; Jing, X.; Wang, F. *Adv. Mater.* **2011**, *23*, 3570−3574.
(58) Cebrián, C.; Mauro, M.; Kourkoulos, D.; Mercandelli, P.; Hertel, D.; Meerholz, K.; Strassert, C. A.; Cola, L. D. *Adv. Mater.* **2013**, *25*, 437−442.
(59) Cheng, G.; Chen, Y.; Yang, C.; Lu, W.; Che, C.-M. *Chem.—Asian J.* **2012**, *8*, 1754−1759.
(60) Cheng, G.; Chow, P.-K.; Kui, S. C. F.; Kwok, C.-C.; Che, C.-M. *Adv. Mater.* **2013**, DOI: 10.1002/adma.301202408.
(61) Kaufmann, G. B.; Cowan, D. O. *Inorg. Synth.* **1960**, *6*, 211−215.
(62) Blessing, R. H. *Acta Cryst., Sect. A: Found. Crystallogr.* **1995**, *51*, 33−38.
(63) Sheldrick, G. M. *SHELXTL, Version 5.1*; Bruker Analytical X-ray Systems, Inc.: Madison, WI, 1997.
(64) Frisch, M. J.; Trucks, G. W.; Schlegel, H. B.; Scuseria, G. E.; Robb, M. A.; Cheeseman, J. R.; Montgomery Jr., J. A.; Vreven, T.; Kudin, K. N.; Burant, J. C.; Millam, J. M.; Iyengar, S. S.; Tomasi, J.; Barone, V.; Mennucci, B.; Cossi, M.; Scalmani, G.; Rega, N.; Petersson, G. A.; Nakatsuji, H.; Hada, M.; Ehara, M.; Toyota, K.; Fukuda, R.; Hasegawa, J.; Ishida, M.; Nakajima, T.; Honda, Y.; Kitao, O.; Nakai, H.; Klene, M.; Li, X.; Knox, J. E.; Hratchian, H. P.; Cross, J. B.; Adamo, C.; Jaramillo, J.; Gomperts, R.; Stratmann, R. E.; Yazyev, O.; Austin, A. J.; Cammi, R.; Pomelli, C.; Ochterski, J. W.; Ayala, P. Y.; Morokuma, K.; Voth, G. A.; Salvador, P.; Dannenberg, J. J.; Zakrzewski, V. G.; Dapprich, S.; Daniels, A. D.; Strain, M. C.; Farkas, O.; Malick, D. K.; Rabuck, A. D.; Raghavachari, K.; Foresman, J. B.; Ortiz, J. V.; Cui, Q.; Baboul, A. G.; Clifford, S.; Cioslowski, J.; Stefanov, B. B.; Liu, G.; Liashenko, A.; Piskorz, P.; Komaromi, I.; Martin, R. L.; Fox, D. J.; Keith, T.; Ai-Laham, M. A.; Peng, C. Y.; Nanayakkara, A.; Challacombe, M.; Gill, P. M. W.; Johnson, B.; Chen, W.; Wong, M. W.; Gonzalez, C.; Pople, J. A. *Gaussian 03,* Revision B.01, Gaussian Inc., Wallingford, CT, 2003.
(65) Hay, P. J.; Wadt, W. R. *J. Chem. Phys.* **1985**, *82*, 270−283.

(66) Wadt, W. R.; Hay, P. J. *J. Chem. Phys.* **1985**, *82*, 284−298.
(67) Hay, P. J.; Wadt, W. R. *J. Chem. Phys.* **1985**, *82*, 299−310.
(68) Tenderholt, A. *PyMOlyze, 2.0*; Stanford University: Stanford, CA, 2005.